Hybridization of Local Exciton and Charge-Transfer States Reduces Non-Radiative Voltage Losses in Organic Solar Cells

Flurin D. Eisner[#], Mohammed Azzouzi[#], Zhuping Fei, Xueyan Hou, Thomas D. Anthopoulos, T. John S. Dennis, Martin Heeney, Jenny Nelson**

Flurin D. Eisner, Mohammed Azzouzi, Prof. Thomas Anthopoulos, Prof. Jenny Nelson
Department of Physics and The Centre for Plastic Electronics
Imperial College London, SW7 2AZ, UK

Dr. Zhuping Fei, Prof. M. Heeney
Department of Chemistry and the Centre for Plastic Electronics
Imperial College London, London SW7 2AZ, UK

Xueyan Hou, T. John. S. Dennis
School of Physics and Astronomy,
Quuen Mary University of London, E1 4NS

Prof. Thomas D. Anthopoulos
King Abdullah University of Science and Technology (KAUST),
KAUST Solar Center, Division of Physical Sciences and Engineering
Thuwal 23955-6900, Saudi Arabia

Dr. Zhuping Fei
Institute of Molecular Plus, Tianjin Key Laboratory of Molecular Optoelectronic Science, Tianjin University, Tianjin, 300072, P. R. China

[#] These authors contributed equally

[*] Corresponding Authors

Abstract

A number of recent studies have shown that the non-radiative voltage losses in organic solar cells can be suppressed in systems with low energetic offsets between donor and acceptor molecular states, but the physical reasons underpinning this remain unclear. Here, we present a systematic study of 18 different donor:acceptor blends to determine the effect that energetic offset has on both radiative and non-radiative recombination of the charge transfer (CT) state. We find that for certain blends, low offsets result in hybridization between charge-transfer and lowest donor or acceptor exciton states, which leads to a strong suppression in the non-radiative voltage loss to values as low as 0.23V associated with an increase in the luminescence of the CT state. Further, we extend a two-state CT-state recombination model to include the interaction between CT and first excited states, which allows us to explain the low non-radiative voltage losses as an increase in the effective CT to ground state oscillator strength due to the intensity borrowing mechanism. We show that low non-radiative voltage losses can be achieved in material combinations with a strong electronic coupling between CT and first excited states, and where the lower band gap material has a high oscillator strength for transitions from the excited state to the ground state. Finally, from our model we propose that achieving very low non-radiative voltage losses may come at a cost of higher overall recombination rates, which may help to explain the generally lower FF and EQE of highly hybridized systems.

Introduction

Bulk-heterojunction organic solar cells have seen a rapid improvement in device performance in the last few years, with power conversion efficiencies (PCE) rising to around 14-15% for single junction solar cells[1-6] and 17% for tandem cells[7], largely driven by the development of new non-fullerene acceptors. In addition to extending the absorption range of BHJ-OSCs, this new class of acceptors has allowed for a large improvement in the open circuit voltage (V_{oc}) without significantly affecting the charge generation efficiency; the mechanism behind this improvement, however, is not yet well understood.[8-10]

Because of the low dielectric constant of organic semiconductors, a photoexcitation on the donor (D) or at the acceptor (A) leads to the formation of a strongly bound singlet exciton (S_1), also known as a local excitation (LE), whose coulombic binding energy needs to be overcome in order to generate free charges. It is generally accepted that for this process to proceed efficiently a heterointerface is required between two materials with appropriate energetic offsets in their oxidation and reduction potentials, or in the energy of their frontier molecular orbitals. [11-13] Many studies have shown that the free charge generation process at the heterointerface then proceeds through the dissociation of the singlet exciton via the formation of an intermediate charge-transfer (CT) state formed at the D-A interface.[14-16]

Until recently, it has been widely believed that in order to achieve efficient dissociation of the CT state into free charges, a minimum Gibbs free energy offset (also known as the driving energy, $\Delta G_{S_1,CT}$) in the CT-state and S_1 state energies is required, thus limiting the maximum achievable open circuit voltage (V_{oc}) [17-19] for any given optical absorption threshold. This necessary driving energy was believed to be around 0.3 eV[14], and only very few fullerene-based solar cells achieved relatively efficient charge generation with a smaller offset. [19-21] However, with the recent development of an increasing number of non-fullerene D-A combinations which show relatively efficient charge generation despite a very small apparent $\Delta G_{S_1,CT}$[9-10, 22-26], it has become increasingly clear that the particular role that the nature and energetics of CT states play in the photogeneration of free carriers needs to be re-evaluated.

Currently, the understanding is that the formation of free charges from CT states is in direct competition with the radiative and non-radiative recombination of the bound electron-hole pair to the ground state.[14, 27-33] The V_{oc} in a D:A organic solar cell is thus determined by the optical gap ($E_{g,opt}$), by $\Delta G_{S_1,CT}$, and by the magnitude of the potential loss due to the

radiative and non-radiative recombination pathways. Due to the reciprocity between light absorption and emission in a solar cell, the highest possible V_{oc} in a D-A solar cell is achieved when the CT state decays only radiatively, which is quantified by the equation

$$V_{oc} = V_{oc,rad} - \Delta V_{oc,nrad} \qquad (1)$$
$$= V_{oc,rad} - \frac{kT}{q}\ln\left(\frac{1}{QE_{EL}}\right),$$

where $V_{oc,rad}$ is the V_{oc} when there is only radiative recombination, $\Delta V_{oc,nrad}$ is the non-radiative voltage loss contribution, and QE_{EL} is the electroluminescence quantum efficiency of the cell. Since QE_{EL} is typically on the order of around 10^{-6}, non-radiative recombination losses in organic solar have traditionally been high (> 350mV).[34]

One way that has been suggested to reduce the non-radiative recombination loss for a given optical gap is to raise the energy of the CT state, by minimizing the energetic offset between the frontier molecular orbitals of the donor and acceptor.[35] This was based on the reasoning that a decreased overlap of the vibrational wavefunction of CT and ground states leads to a suppression of the non-radiative recombination pathway. It was also suggested that the large spacing of vibrational states in organic semiconductors means that a relatively high level of non-radiative recombination is inevitable in such cells. While the findings of Reference [35] appear to be relatively successful in predicting the trend in non-radiative voltage losses of fullerene-based D-A blends with high driving energies, many recent D-A blends with very low $\Delta G_{S_1,CT}$ have achieved non-radiative voltage losses that are on the order of 100 meV lower than might be expected from their CT-state energy given the trends shown by the majority of donor:acceptor systems[24, 36-37], for reasons which are not yet clear. One explanation that has been suggested is that non-radiative recombination in low $\Delta G_{S_1,CT}$ blends is determined not by the emission properties of the CT state but rather by those of the S_1 state, and that low non-radiative recombination can therefore be achieved by using materials with high luminescence yield[36, 38] (through equation 1). This was reasoned on the basis that highly luminescent S_1 states can increase the luminescence of the CT state through the intensity borrowing mechanism for low $\Delta G_{S_1,CT}$ blends. This mechanism had also been previously proposed to explain the strong luminesce properties of low $\Delta G_{S_1,CT}$ D-A molecules[39-40] and has been computationally predicted for several polymer:fullerene blends[41-43].

Whilst the findings of reference [36], and of other recent studies on low $\Delta G_{S_1,CT}$ blends[38, 44], are an important step forward in understanding the role that CT states play in governing the charge generation in small $\Delta G_{S_1,CT_0}$ D-A solar cells, the fundamental question of the link between the small $\Delta G_{S_1,CT_0}$ and low non-radiative losses is as yet not properly understood.

In this contribution, , through a systematic study using a series of increasingly fluorinated poly[(2,6-(4,8-bis(5-(2-ethylhexyl)thiophen-2-yl)-benzo[1,2-b:4,5-b′]dithiophene))-alt-(5,5-(1′,3′-di-2-thienyl-5′,7′-bis(2-ethylhexyl)benzo[1′,2′-c:4′,5′-c′]dithiophene-4,8-dione)] (PBDB-T) donors in conjunction with a variety of fullerene and non-fullerene acceptors. First, we show that by depressing both the highest occupied molecular orbital (HOMO) and lowest unoccupied molecular orbital (LUMO) through fluorination of the donor, the energy of the donor-acceptor CT state can be effectively moved closer to the first excited state. Second, by performing a detailed voltage loss analysis of the various blends we find that the non-radiative voltage losses do not reduce linearly with increasing CT state energies; instead, non-radiative voltage losses are minimised, reaching values as low as 0.23 V, for systems where the CT state and first excited state energies are very close. We suggest that this reduced non-radiative voltage loss results from the hybridization of the CT state with the first excited state and the effect of this hybridisation on the CT state oscillator strength. Finally, using a recent new model to quantify the non-radiative voltage losses[37], we simulate the observed behaviour through an increase in both the CT state energy and the effective oscillator strength of the CT state to ground state transition. We discuss how control of the CT state properties could lead to lower voltage losses and higher performance in organic heterojunction solar cells.

Experimental Results

Materials

Our study is based on three PBDB-T based polymers as the donor (D) component in our BHJ cells, which have been fluorinated to different extents in order to modulate their energy levels. PBDB-T[45], which we will refer to as D-0F from here onwards, is a well-known donor polymer which was amongst the first polymers to outperform fullerene-based solar cells with non-fullerene small molecule acceptors, and its derivates have been used in some of the highest performing organic solar cells to date[3-4, 46]. To complement PBDB-T, we use the recently reported PFBDB-T polymer, in which the thiophenes flanking the electron deficient benzo[1′,2′-c:4′,5′-c′]dithiophene-4,8-dione are mono-fluorinated, and P4FBDB-T, in which a further two fluorine atoms are attached to the benzodithiophene unit (Figure 1). We will refer

to these polymers as D-2F and D-4F, respectively. The effect of the fluorination is to increase the oxidation potential as measured by cyclic voltammetry. Referencing against ferrocene allows the HOMO energy levels to be approximated, and they decrease from -5.33eV to -5.46eV and -5.63eV from D-0F to D-2F and D-4F respectively, without significantly affecting the band gap (Table S1), as extracted from cyclic voltammetry (CV) measurements.

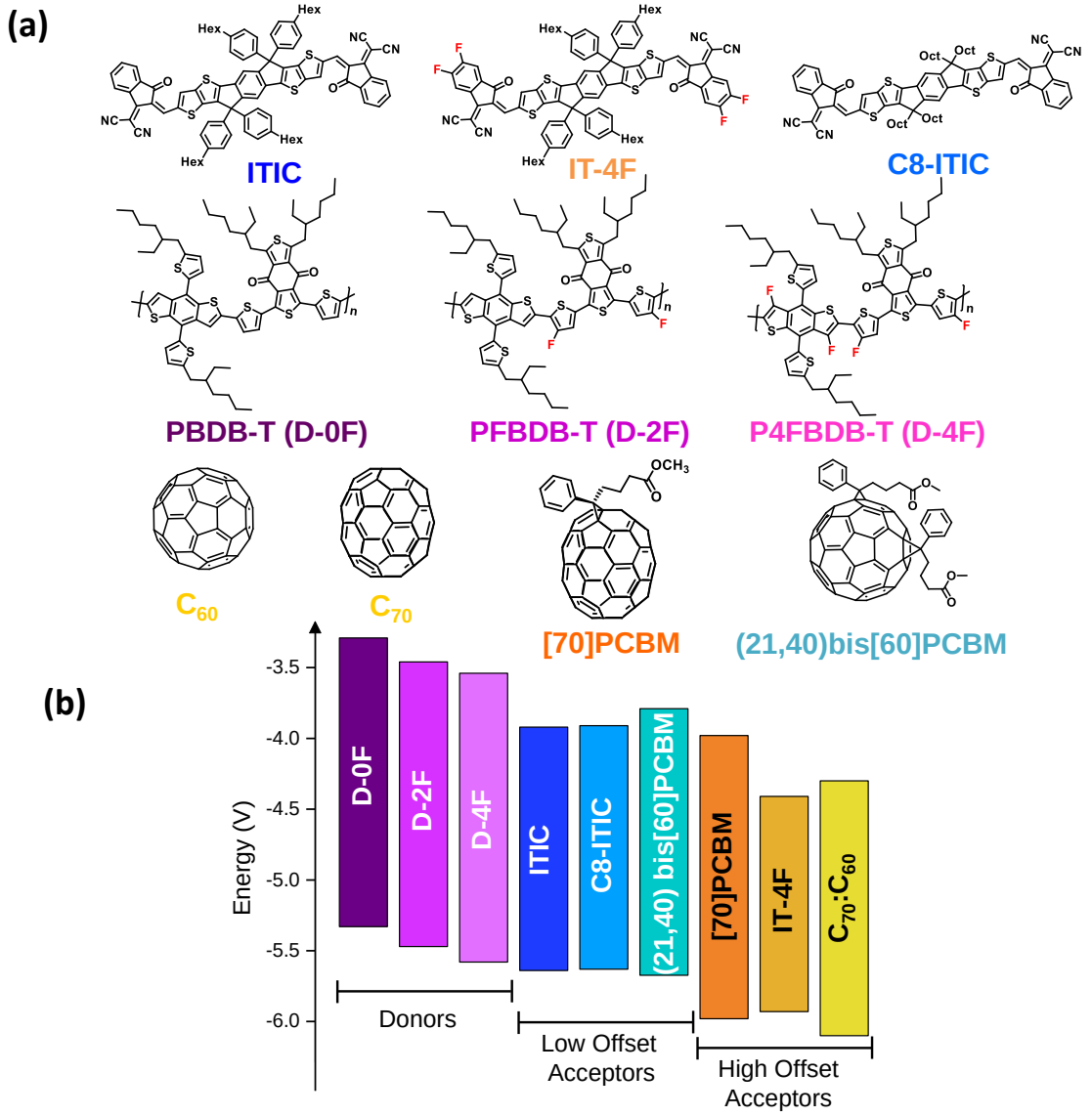

Figure 1: **Materials and Energy Levels** a) Molecular structures of the materials used in the study. b) HOMO and LUMO energies (estimated from cyclic-voltammetry measurements) of the materials (see Supplementary Figure 1).

We note that since energy levels extracted from CV measurements can be subject to relatively large errors, we performed additional checks of the trend using both air photo-

emission spectroscopy (APS) and using DFT calculations, both of which confirmed the trend in the energy levels extracted from CV (Table S1).

In conjunction with these three polymers, we use three different previously reported ITIC-based non-fullerene acceptors, ITIC[46-47], C8-ITIC[5] and IT-4F[4], and three reported fullerene acceptors, $PC_{71}BM$, a pristine fullerene C_{60}:C_{70} mixture[48], and (21,40)bis[60]PCBM[43], a purified equatorial Bis-PCBM isomer with a deep HOMO compared to [60]PCBM[49-50]. The acceptors in this study were chosen to have a range of driving energies for charge separation when paired with the three donors, both for fullerene and non-fullerene acceptors. Driving energy ($\Delta E_{S_1,CT}$) is defined here as the difference in the energy of the lowest singlet exciton state (E_{S_1}) (approximately equal to the band gap of the lower band gap material) and the lowest CT state energy (E_{CT}) of the D-A blend, and is used as an approximation for the difference in Gibbs free energy of the exciton and CT states. This approximation ignores the effects of the density of CT relative to exciton states, which contributes to the entropic term in the Gibbs free energy, and energetic disorder, which affects the relationship between the state energy difference and the Gibbs free energy.[51] $\Delta E_{S_1,CT}$ is generally assumed to be correlated to either the difference in the HOMO energies of the donor and the acceptor ($\Delta E_{HOMO} = E_{HOMO,D} - E_{HOMO,A}$) or the difference in LUMO energies ($\Delta E_{LUMO} = E_{LUMO,D} - E_{LUMO,A}$), whichever is the lower. Taking this approximation, by examining the energetics of the materials studied here (Figure 1b) we expect D-A blends with ITIC, C8-ITIC and (21,40)bis[60]PCBM to result in low $\Delta E_{S_1,CT}$ when paired with D-2F and D-4F, whilst the other acceptors should still have a substantial $\Delta E_{S_1,CT}$ even when paired with D-4F. It is worth noting that the expected $\Delta E_{S_1,CT}$ approaches zero in blends of ITIC, C8-ITIC and (21,40)bis[60]PCBM with D-4F. Finally, we would like to comment that by using three donors with the same backbone the number of molecular parameters that are likely to change between them is smaller than by using three completely structurally different donors. This reduces the number of variables that change from one blend to another and should allow for a more consistent and reliable study on the effects that the energetics of the blends play in determining the recombination dynamics of the CT state.

Device Performance

Figure 2 plots the averaged V_{oc} and PCE under simulated AM1.5 illumination of all donor-acceptor combinations against the HOMO levels of the donors as calculated from the C-

V measurements. All devices were fabricated in the so-called inverted solar cell architecture, ITO/ZnO/Active Layer/MoO_3/Ag, and all were processed without additives. Each data point is the average of at least 24 cells. The full device parameters for all blends are shown in Table 1 and can also be found in Figure S2.

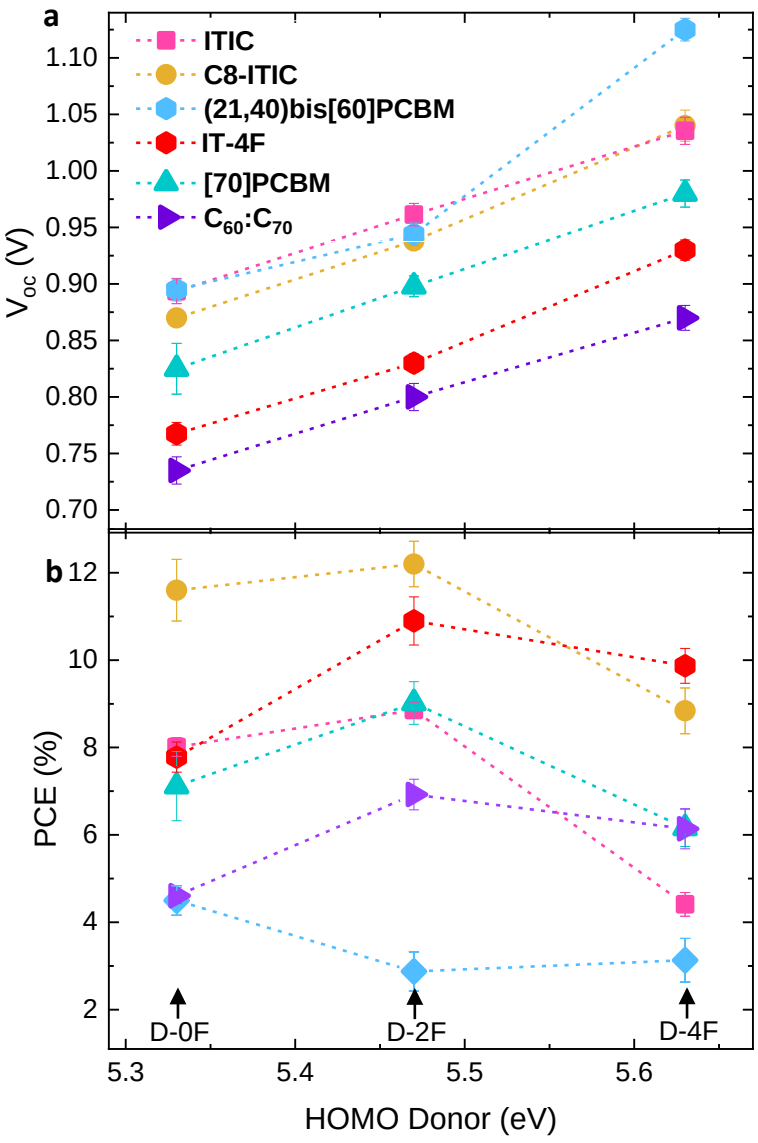

Figure 2: **Device parameters from current density-voltage measurements**. The a) open-circuit voltages and b) power-conversion efficiencies of all studied blends are plotted against the HOMO level of the donor in the blend. Each acceptor series (blended with D-0F, D-2F and D-4F) is plotted in a different colour. The error in the energy levels are $\pm 0.05eV$, and are not shown as error bars for clarity.

Donor	Acceptor	FF	V_{oc} (V)	Jsc ($mAcm^{-2}$)	PCE (%)
D-0F	C8-ITIC	0.68	0.87	19.3	11.6
D-2F	C8-ITIC	0.69	0.94	18.8	12.2
D-4F	C8-ITIC	0.58	1.04	14.6	8.8
D-0F	ITIC	0.54	0.89	16.5	8.0
D-2F	ITIC	0.60	0.96	16.8	8.9
D-4F	ITIC	0.44	1.04	14.1	4.4
D-0F	IT-4F	0.62	0.77	16.4	7.8
D-2F	IT-4F	0.67	0.83	19.6	10.9
D-4F	IT-4F	0.62	0.93	18.4	9.9
D-0F	(21,40)-Bis[60]PCBM	0.53	0.90	9.6	4.5
D-2F	(21,40)-Bis[60]PCBM	0.35	0.94	8.7	2.9
D-4F	(21,40)-Bis[60]PCBM	0.47	1.13	6.0	3.1
D-0F	[70]PCBM	0.63	0.83	13.8	7.1
D-2F	[70]PCBM	0.67	0.90	15.0	9.0
D-4F	[70]PCBM	0.59	0.98	10.6	6.2
D-0F	$C_{60}C_{70}$	0.62	0.74	10.1	4.6
D-2F	$C_{60}C_{70}$	0.66	0.80	13.2	6.9
D-4F	$C_{60}C_{70}$	0.62	0.87	11.4	6.1

Table 1. Average device parameters from current-voltage measurements under AM 1.5 illumination for all the studied blends.

As expected, the V_{oc} (Figure 2a), increases roughly linearly with the donor HOMO for each acceptor series. The difference between the V_{oc} of blends with D-0F and with D-4F is in the region of 0.14-0.22V for all acceptor series, although there is significant scatter between influence of the HOMO donor on the V_{oc} between the different acceptors. Three acceptors (ITIC, C8-ITIC, (21,40)bis[60]PCBM) achieve a V_{oc} greater than 1V with D-4F, and the other three (IT-4F, [70]PCBM, C60C_{70}) achieve maximum V_{oc} values around 0.95V or lower.

In terms of the obtained PCEs, blends with D-2F generally show the best performance, due to the higher fill factor (FF) and short-circuit current (J_{sc}) relative to blends with either D-0F or D-4F (Figure S2). The improvement over D-0F may be partly due to the enhancement of dipole moments and possible improved morphology upon fluorination leading to better charge extraction[52-53], in addition to the increase in the V_{oc}. In contrast devices with D-4F displayed poorer FF and J_{sc} compared to devices with D-2F, leading to lower PCE despite higher V_{oc}. The fact that FF and J_{sc} are reduced for all D-4F:acceptor combinations, even for cases with a sufficiently high ΔE_{HOMO} for efficient charge generation (IT-4F, [70]PCBM and C_{60}:C_{70}), suggests that at least part of this charge generation loss is due to 'over- fluorination', which leads to a reduction in the solubility of the donor in the solvent and hence an adverse effect on

the formation of donor crystallites and a sub-optimal film morphology.[54-57] Nonetheless, despite the lower device performance, it is interesting to note that even the D-4F devices with C8-ITIC, ITIC and (21,40)bis[60]PCBM) can achieve a reasonably high external quantum efficiency (EQE) values despite negligible donor-acceptor HOMO offsets (Figure S3), with D-4F:C8-ITIC achieving EQE values over 70%, with a PCE over 9%.

Energetics of the Molecular States

In order to gain insight into the effect that shifting the HOMO of the donor has on the relative energetics of excitonic and CT states in the blends, we performed high-dynamic-range EQE and electroluminescence (EL) measurements on complete devices. **Figure 3a-c** compares the sub-band gap EQE and EL spectra for D:A series using three different acceptors, with purple, red and green lines denoting D-0F:A, D-2F:A and D-4F:A blends, and the yellow lines showing the spectra from pristine lowest band gap material. The three acceptors were chosen as representatives for systems with small $\Delta E_{S_1,CT}$ (C8-ITIC), intermediate $\Delta E_{S_1,CT}$ (IT-4F), and large $\Delta E_{S_1,CT}$ ([70]PCBM), in Figs 3a, b and c, respectively. The spectra for the other material combinations used in this study are shown in Figure S6. We note that similarly low injection currents were applied in all the EL spectra shown, and that injection currents were kept constant for each acceptor series. The effects of injection current on EL emission spectra are shown in Figure S7.

For all blend devices with D-0F the sub-band gap EQE spectra (lines and symbols) show a clear additional absorption at low energies, that is not observed in the spectra of the pristine materials. The sub-band gap absorption tail occurs over a similar energy range to the peak of the EL spectrum in each case, suggesting that this feature results from the absorption of a CT state which is located at a significantly lower energy (E_{CT}) than the first excited singlet state (E_{S_1}). This is in agreement with expectations from examination of the energy level of the materials (Figure 1b).

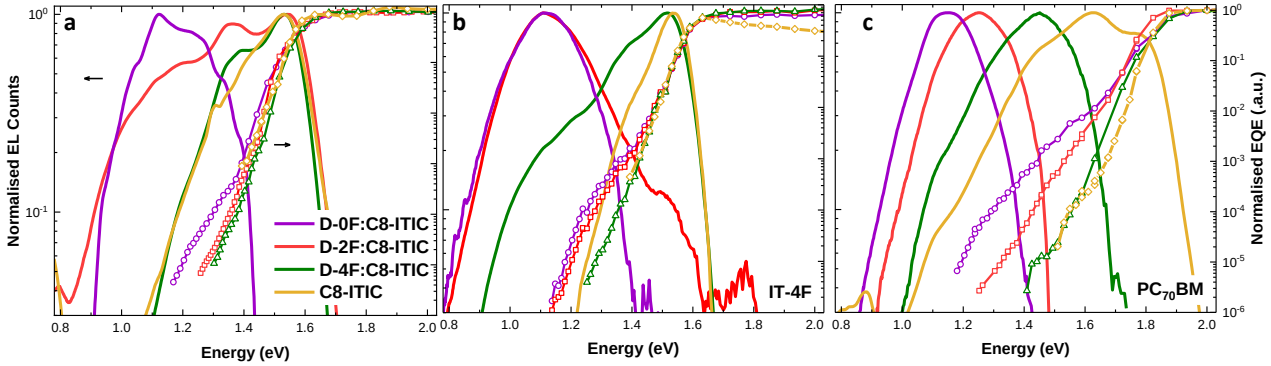

Figure 3: **Electroluminescence (EL) and external quantum efficiency measurements (EQE) on devices**. Normalized EL and EQE spectra of the three donors paired with three different acceptors representing low offset (a), medium offset (b) and high offset (c) cases in C8-ITIC, IT-4F and [70]PCBM, respectively. The pristine spectrum of the lowest band gap material in each case is plotted in yellow.

Turning to the spectra of acceptors with D-2F, which has a deeper HOMO compared to D-0F, blends with this donor exhibit a sub-band gap absorption feature in the EQE that is blue shifted compared to that observed in D-0F blends. The strongest blue-shift is observed in the blend with C8-ITIC, where the CT-state absorption appears to overlap significantly with the absorption of the C8-ITIC singlet state (blue line). This is also reflected in the correspondingly large blue-shift of D-2F:C8-ITIC compared to D-0F:C8-ITIC in the EL CT-emission of this blend. Additionally, D-2F:C8-ITIC also appears to contain a significant contribution from the pristine C8-ITIC singlet emission. Interestingly, this large overlap in the CT-state absorption with the S_1 absorption in blends with D-2F, coupled with a substantial EL contribution from the lowest band gap pristine material, is also present in the other acceptor blends with low $\Delta E_{S_1,CT}$ i.e. ITIC and (21,40)bis[60]PCBM (Figure S6). In contrast to D-2F:C8-ITIC, both D-2F:IT-4F and D-2F:[70]PCBM show a much weaker blue-shift in CT-state absorption in the EQE compared to the corresponding D-0F blends and a correspondingly small blue-shift in CT emission which show little or no contribution from the S_1 emission.

Finally, in blends with D-4F, the donor with the deepest HOMO, a significant further blue-shift of the EQE absorption tail (compared to blends with D-0F and D-2F) is observed in all cases, to the extent that for D-4F:C8-ITIC and D-4F:IT-4F the EQE tail of the blend overlaps almost completely with that of the pristine acceptor EQE. Mirroring this behaviour, the EL emission spectrum for D4:C8-ITIC is almost completely indistinguishable from the pristine

C8-ITIC emission, whilst the D-4F:IT-4F emission now contains a significant contribution from the pristine IT-4F emission. Complete overlap between blend and pristine spectra is also observed with the other two blends with very low $\Delta E_{S_1,CT}$, D-4F:ITIC and D-4F:(21,40)bis[60]PCBM, both of which also exhibit blend sub-band gap EQE spectra which overlap with the EQE spectrum of the lowest-band gap pristine component (Figure S6) (S_1 absorption). By contrast, the EL spectra of D-4F:[70]PCBM, and also D-4F:C_{60}:C_{70}, are noticably blue-shifted compared to blends with D-2F, but emission from the CT-state can be clearly distinguished from that of the S_1 emission.

Based on the above behaviour of the blends in the different acceptors, we can split the acceptors into three different groups. Firstly, acceptors with large $\Delta E_{S_1,CT}$ when paired with all donors, which show no mixing between CT and singlet states with any of the donors. Secondly, acceptors with large $\Delta E_{S_1,CT}$ but which show partial mixing when paired with D-4F, and thirdly, acceptors with low $\Delta E_{S_1,CT}$ when paired with deep HOMO donors which show partial mixing between CT and singlet states when blended with D-2F and almost complete mixing when blended with D-4F. [70]PCBM and C_{60}:C_{70} fall into the first category, IT-4F falls into the second category, and ITIC, C8-ITIC and (21,40)bis[60]PCBM fall into this last category. We will now examine the voltage losses exhibit by each of these category of blends in more detail.

Trends in Energy Losses

The accurate determination of CT and singlet state energies has been a matter of debate in the community[58-59], and different definitions exist[14]. For consistency, and to avoid confusion, we will define the energies of states here by their electroluminescence spectra at room temperature, without considering the effects of disorder on the determination of the energies.[14, 59]We will refer to the photon energy at which the CT EL emission peaks as the CT state energy E_{CT}, and similarly the photon energy at which the S_1 EL emission peaks as the singlet excited state energy $E_{S_1,}$ from here onwards. Determining E_{CT} is relatively simple for cases where the CT state is completely uncoupled from S_1, but more difficult for the cases of high spectral overlap of CT and S_1 emission, such as for D-4F:C8-ITIC (Figure 3a). In order to approximate E_{CT}, we fit the normalised EL spectra with a Gaussian function multiplied by E^3 (equation S1), which can include contributions from both singlet and vibronic CT state modes. More information can be found in the supplementary information. Note that for CT values very close to S_1 the

error on E_{CT} may remain fairly large due to the uncertainty in separating the CT state emission from the singlet exciton emission when there is a high overlap between blend and pristine spectra, and the values obtained are estimates only.

Using the above method allows us to estimate the driving energy for CT-state dissociation, $\Delta E_{S_1,CT}$, for our studied blends, as the energetic difference between E_{CT} and E_{S_1}. A resultant plot of V_{oc} against $\Delta E_{S_1,CT}$ (Figure S9), however, is not very informative other than to note the significant scatter around a linear variation of V_{oc} with $\Delta E_{S_1,CT}$, suggestive of CT-state properties other than energy having a significant impact on the attainable V_{oc}, as has been previously noted.[37] Instead, it is more useful to break down the separate energy losses due to non-radiative and radiative recombination, which we calculate in the same way as presented by Yao et al.[34], by invoking the reciprocity between light absorption and emission in a solar cell.

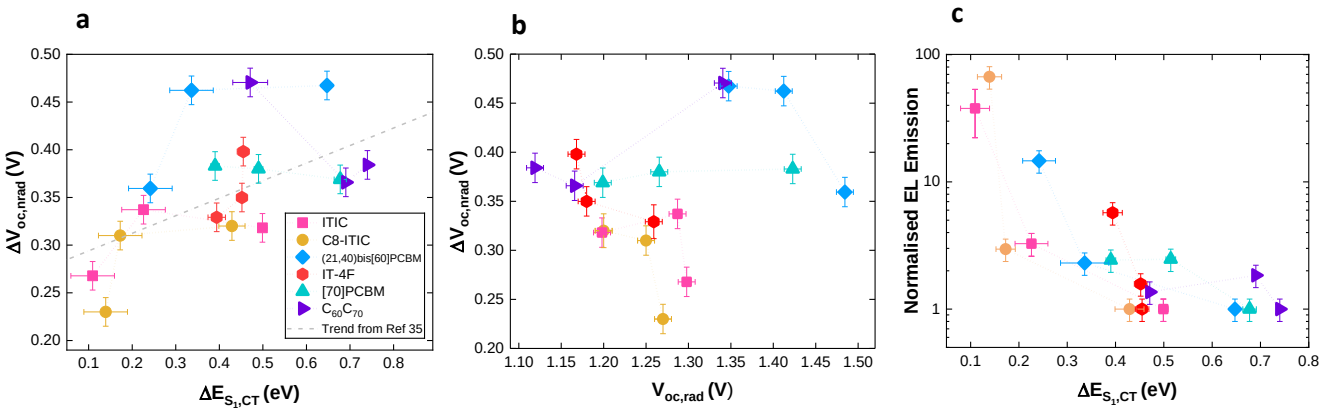

Figure 4: **Experimental non-radiative voltage losses as a function of driving energy**. The non-radiative voltage loss $\Delta V_{oc,nrad}$ as calculated from EL and EQE measurements for every studied blend is plotted against (a) the driving energy $\Delta E_{S_1,CT}$ and (b) the open circuit voltage in the radiative limit, $V_{oc,rad}$. In (a), the expected trend considering only the effect of the change in CT-state energy (i.e. trend from Ref 35) for the case of a blend with $E_{S_1} \approx 1.6$eV is also plotted. c) the EL emission intensity normalized with the emission from the blend with D-0F for each acceptor series. The EL emission spectra were measured with injection currents of 22 mAcm^{-2} for blends with C8-ITIC and ITIC, 55 mAcm^{-2} for blends with (21,40)bis[60]PCBM, [70]PCBM and IT-4F, and 110 mAcm^{-2} for blends with C_{60}:C_{70}.

In Figure 4a we plot the energy losses due to non-radiative recombination, $\Delta V_{oc,nrad}$ against $\Delta E_{S_1,CT}$ for all of the studied blends. Also shown is the empirical relationship between $\Delta V_{oc,nrad}$ and ΔE_{CT} based on a large number of fullerene based BHJ cells, introduced by Benduhn et al.[35], which takes the form $\Delta V_{oc,nrad} = 0.547V - 0.184VeV^{-1}(E_{CT} - \lambda)$, where λ is the low-frequency reorganization energy, for a blend with E_{S_1} at 1.6eV (similar to C8-ITIC). We note that our definition of E_{CT} differs from other definitions in the literature,

such as in Benduhn et al.[35], by approximately λ, i.e. $E_{CT} = E_{CT^*} - \lambda$, where E_{CT^*} is the commonly used definition of the energy of the CT-state. The magnitude of λ is commonly on the order of 100 meV for organic BHJ blends.[60] Clearly, the data suggests that it is insufficient to take only the energy of the CT state into consideration when predicting $q\Delta V_{oc,nrad}$, with a large degree of scatter around a general trend of decreasing $q\Delta V_{oc,nrad}$ with decreasing $\Delta E_{S_1,CT}$, and some acceptor series (e.g. [70]PCBM) even showing an increase in $q\Delta V_{oc,nrad}$ with decreasing ΔE_{S_1-CT}. Whilst there are evidently many factors involved in explaining the various trends exhibited by the various acceptor series, we wish to focus on the particularly consistent behaviour displayed by three of the blends, namely the sharp decrease in $q\Delta V_{oc,nrad}$ of D-4F blends with ITIC, C8-ITIC and (21,40)bis[60]PCBM compared to their blends with D-2F, which is not exhibited by any of the other acceptor materials. This trend is of particular importance since the behaviour of low-offset materials has been the focus of much recent attention in the literature. [8, 26, 36, 44] In order to explain this trend, we turn to the sub-band gap EQE and EL results (Figure 3), and note that from the qualitative study of this figure we identified three acceptor materials which formed highly hybridized CT and E_{S1} states when blended with D-4F, namely ITIC, C8-ITIC and (21,40)bis[60]PCBM, which are the same blends which exhibit the strong reduction in $q\Delta V_{oc,nrad}$. In particular, the blends with the lowest ΔE_{S_1-CT}, D-4F:C8-ITIC and D-4F:ITIC display extremely low $\Delta V_{oc,nrad}$ values of 0.23 and 0.27eV, respectively, and have EL spectra in which CT and S_1 emission cannot be distinguished.

The correlation between a sharp decrease in $q\Delta V_{oc,nrad}$ from Figure 4a, and an increase in the mixing of CT and S_1 EL emission provides a strong indication that the two phenomena are related. However, we have previously noted that defining E_{CT} from the EL spectra is subject to a relatively large error, especially for highly hybridized systems, and it is more reliable to analyse the data in terms of $V_{oc,rad}$, which can be directly calculated from EL and EQE measurements on blend devices, and so reflects the true interfacial energetics in the device[34]. $V_{oc,rad}$ is also a more useful quantity than $\Delta E_{S_1,CT}$, since it contains information not only on E_{CT} but also on the absorption coefficient, density and oscillator strength of the CT states.[37] The relationship between the extracted values of $\Delta E_{S_1,CT}$ and $V_{oc,rad}$ can be found in Figure S11. A resulting plot of $\Delta V_{oc,nrad}$ against $V_{oc,rad}$ is shown in Figure 4b. The general trends observed from Figure 4a are replicated with a large decrease in $\Delta V_{oc,nrad}(V_{oc,rad})$ in D-4F blends compared to D-2F for highly hybridized blends, which is not realised in the other blends.

Since the two Figures show qualitatively the same trend, the same analysis as above can be applied to Figure 4b as to Figure 4a.

Low $\Delta E_{S_1,CT}$ in D-A blends, along with a highly luminescent low-gap component, has recently been identified as key requirement for low $\Delta V_{oc,nrad}$ values in conjunction with a high charge generation efficiency.[36] Consequently, in Figure 4c we plot the peak EL emission of all of the blends studied as a function of $\Delta E_{S_1,CT}$ normalized to the magnitude of the D1-0F:acceptor emission of each blend. As in previous studies [36], there is an increase in the EL emission as $\Delta E_{S_1,CT}$ becomes small, with a strong increase in emission as $\Delta E_{S_1,CT}$ decreases below 0.4eV. It is particularly interesting to note that the largest increases in emission are associated with the largest decreases in $V_{oc,nrad}$ from Figure 4b.

Non-Radiative Recombination in a Two-State Model

In order to explain the trends in our data, we will now draw upon and extend a model of the non-radiative properties of CT states that we have recently introduced.[37] This model is based on the approach introduced by Jortner *et al.*[61] for donor-acceptor complexes in solution, which was developed into a model for non-radiative recombination in organic heterojunctions by Benduhn et al., [35] and concerns a two-level system involving a CT state and a ground state. Using this approach, we were able to determine the relationship between $\Delta V_{oc,nrad}$ and $V_{oc,rad}$ as a function of various material parameters, such as the difference in Gibbs free energy between the two states, $\Delta G_{S_1,CT}$, the high and low frequency reorganization energies, the oscillator strength of the CT to ground state transition, the difference in static dipole moments of the states, the CT-state energy and the CT-state density. We were able to show that the strength of non-radiative recombination is controlled not only by the CT state energy, but also by other CT-state properties, and the energy gap law (EGL) is not always obeyed. For a full derivation and explanation of the model the reader is referred to reference [37].

We thus attempt to explain our experimental results for the relationship between $\Delta V_{oc,nrad}$ and $V_{oc,rad}$ (Figures 4a,b) and the trends in peak EL intensity (Figure 4c) within the context of this basic model. We will focus our attention on explaining the most important feature of the observed V_{oc} in our series of devices, namely the large reduction in ΔV_{oc}^{nrad} observed for blends with D-4F with ITIC, C8-ITIC and (21,40)bis[60]PCBM. The behaviour of the other acceptor series is discussed in the supplementary information.

We firstly reiterate three important findings from the experimental (EQE and EL) results: 1) the observed decrease in $\Delta V_{oc,nrad}$ with D-4F occurs for blends where a large level of mixing, identified from the resonance of CT and exciton emission energies, is observed, and not for the other blends; 2) large decreases in $\Delta V_{oc,nrad}$ at low $\Delta E_{S_1,CT}$ are accompanied by a large increase in the EL intensity and 3) the increases in E_{CT} with fluorination from EL and EQE measurements are insufficient by themselves to explain the observed decrease in $\Delta V_{oc,nrad}$[37], according to either the model from reference 35 or 37. We additionally note that the above observed phenomena cannot be explained be large changes in morphology, since there appears to be little change in morphology between D-2F and D-4F blends (Figure S12). In terms of our two-state model[37], the parameters besides an increase in E_{CT} that may bring about a decrease in ΔV_{oc}^{nrad} are an increase in the CT-ground state oscillator strength f_{CT,S_0}, an increase in the difference in static dipole moments between CT and ground states $\Delta\mu_{CT,S_0}$, or decreases in the high or low-frequency reorganization energies, λ_h and λ_l. We note here that previous studies on low $\Delta E_{S_1,CT}$ molecules in solution have found that an increase in the luminescence of the CT state with an associated strong increase in f_{CT,S_0} is due to intensity borrowing from the singlet exciton, enabled by the hybridization of singlet and CT states.[39-40] Therefore, from our experimental findings (1) and (2) (above), we suggest the parameter that is most likely to affect both $\Delta V_{oc,nrad}$ and the high EL intensity for our highly hybridized systems is f_{CT,S_0}.

Additionally, we note that through our two-state model, we can indeed reproduce the steep decrease of ΔV_{oc}^{nrad} by increasing f_{CT,S_0} by two orders of magnitude; however, the physical origin of this increase in oscillator strength is not explained by the two-state model. The remaining question is, therefore, what causes the increase of the oscillator strength of the CT state when the driving energy decreases? In the following section, we draw on previous research into the luminescence of donor-acceptor dyads, to explain the inferred increase in f_{CT,S_0} and subsequent low $\Delta V_{oc,nrad}$ for our low $\Delta E_{S_1,CT}$ blends.

Nonradiative Recombination in a Three-State Model

Bixon et al., have previously demonstrated that an increase in the luminescence intensity with decreasing solvent polarity in some donor-bridge-acceptor molecules can be quantitatively described by accounting for the mixing of local excited singlet and charge transfer states, due to intensity borrowing mechanism from the singlet to ground state transition.[40] Several studies have since used similar approaches to show that CT-state and local excited state mixing also

occurs in organic semiconductor heterojunctions relevant to organic solar cells. [32, 62-63] Based on Bixon's work, we thus introduce a similar three-state model, where a first excited singlet state (also known as a locally excited (LE) state) has been included at an energy E_{S_1}, higher than the zeroth-order CT state energy E_{CT} by an energy $\Delta E_{S_1,CT}$, much higher than the ground state energy E_{S_0} (Figure 5a). The contribution of the spin-related part of the wavefunction to the performance of the device is generally negligible [64], and thus the wavefunctions of the ground state, Ψ_{S_0}, the first excited singlet state Ψ_{S_1}, and first CT state Ψ_{CT}, can be expressed terms of their electronic states $|\phi_{S_0}\rangle, |\phi_{CT}\rangle, |\phi_{S_1}\rangle$ with corresponding vibrational levels $|\alpha\rangle, |\beta\rangle, |\gamma\rangle$ (with energies $\epsilon_\alpha, \epsilon_\beta, \epsilon_\gamma$, respectively). We assume that there is little mixing between the wavefunctions Ψ_{S_1} and Ψ_{S_0} and between Ψ_{CT} and Ψ_{S_0}, which is a reasonable approximation if Ψ_{S_1} is energetically far away from and Ψ_{S_0}, but we allow the wavefunctions of Ψ_{S_1} and Ψ_{CT} to interact. Following the method detailed in the supplementary information, we find that the radiative coupling between the CT state and ground state is then given by

$$\langle \Psi_{S_0}|\hat{\mu}|\Psi_{CT}\rangle = \langle \phi_{S_0}|\hat{\mu}|\phi_{CT}\rangle\langle\alpha|\beta\rangle + \sum_{\gamma} \frac{V_{S_1,CT}\langle\alpha|\gamma\rangle\langle\gamma|\beta\rangle}{E_{S_1} - \hbar\omega_{CT} - \epsilon_\beta + \epsilon_\gamma} \langle \phi_{S_0}|\hat{\mu}|\phi_{S_1}\rangle, \qquad (2)$$

where $\hat{\mu}$ is the electronic dipole operator, and $V_{CT,S_1} = \langle \phi_{CT}|\hat{H}|\phi_{S_1}\rangle$ is the electronic coupling (where $\hat{H}$ is the Hamiltonian of the system), and $\hbar\omega_{CT}$ is the energy of the emitted photon from the lowest CT to ground state transition. Using the definition for the transition dipole moment, $M_{a,b} = \langle \phi_a|\hat{\mu}|\phi_b\rangle$, and assuming small change in the equilibrium geometry between Ψ_{S_0} and Ψ_{S_1} (i.e. approximating $\langle a|\gamma\rangle = \delta_{\alpha\gamma}$), which seems valid given the small Franck-Condon shift observed in these materials, we then find

$$\langle \Psi_{S_0}|\hat{\mu}|\Psi_{CT}\rangle = \left(M_{S_0,CT} + \frac{M_{S_1,S_0}V_{S_1,CT}}{E_{S_1} - \hbar\omega_{avg}}\right)\langle\alpha|\beta\rangle, \qquad (3)$$

This result follows from the analysis in the supplementary information, where, in order for the Franck-Condon approach to be valid, we approximate $\hbar\omega_{CT}$ by the average energy of peak emission $\hbar\omega_{avg}$, following the approximations made in reference [40]. Examining equation 3, we see that the electronic part of the radiative coupling consists of the transition dipole moment between the ground state and the CT state ($M_{S_0,CT}$), with an additional modulation term which depends on the transition dipole moment between the ground and first excited state (M_{S_1,S_0}), the electronic coupling between the first excited state and the CT state $V_{S_1,CT}$, and the difference

in the energy of the singlet state relative to that of the emitted photon. We can thus define a new 'effective' transition dipole moment for the radiative transition between CT state and ground state,

$$M^*_{S_0,CT} = M_{S_0,CT} + \frac{M_{S_1,S_0} V_{S_1,CT}}{E_{S_1} - \hbar\omega_{avg}}. \quad (4)$$

This expression can be used to calculate a radiative rate constant that depends on the interaction between CT state and first excited state.

Finally, following the calculations in the supplementary information, we can define an effective oscillator strength for the CT to ground state transition,

$$M^{*2}_{S_0,CT} \propto f^*_{S_0,CT} = f_{S_0,CT} + \frac{f_{S_1,S_0} V^2_{S_1,CT}}{\Delta E^2_{S_1-CT}} + 2\frac{f^{1/2}_{S_1,S_0} f^{1/2}_{S_0,CT} V_{S_1,CT}}{\Delta E_{S_1-CT}}, \quad (5)$$

where $f^*_{S_0,CT}$ is the effective CT to ground state oscillator strength, $f_{S_0,CT}$ is the CT-ground state oscillator strength in the absence of state mixing, f_{S_0,S_1} is the excited state to ground state oscillator strength, and we have re-introduced the energy offset between the CT and first excited state, ΔE_{S_1-CT}.[39, 65] $f^*_{S_0,CT}$ is therefore strongly dependent on the inverse square of the energetic offset (the driving energy) between the first excited and the CT state, as well as on the square of the electronic coupling between the two states.

In Figure 5b, we plot the ratio $f^*_{S_0,CT}/f_{S_0,CT}$ calculated as a function of $\Delta E_{S_1,CT}$ and the electronic coupling $V_{S_1,CT}$, for a CT oscillator strength in the absence of mixing ($f_{S_0,CT}$) of 2×10^{-2}, and electronic couplings ranging from 10 to 60 meV. Even with only a moderate electronic coupling of 40meV, the oscillator strength is increased by more than an order of magnitude relative to the unhybridised case at a driving energy of 0.1eV, whilst at an electronic coupling of 60meV the oscillator strength is almost 2 orders of magnitude higher. Since the oscillator strength is directly related to the radiative capability of the transition, from equation 5 we expect a high increase in the emission of the CT state with decreasing $\Delta E_{S_1,CT}$ due to intensity borrowing from the $S_1 \rightarrow S_0$ transition, as observed directly in Figure 4c and in previous studies[36].

Effect of Hybridization on Non-Radiative Voltage Loss

Having established a suitable framework for treating the wavefunction overlap of low $\Delta E_{S_1,CT}$ systems, we now turn to explaining the experimental voltage loss behaviour exhibited by the studied blends (Figure 4). Using our expression for the transition dipole moment from the three-state model that incorporates mixing between CT and singlet states (equation 5), we can calculate $\Delta V_{oc,nrad}$ and $V_{oc,rad}$ values within our two-state model. We note in passing that we can show that the generalized two-state Mulliken-Hush formulation relating the electronic coupling to the transition dipole moment is a good approximation for the three-state model (see SI)[66], allowing us to calculate $\Delta V_{oc,nrad}$ and $V_{oc,rad}$ using the same method as previously[37]. Figure 5c and d plot the expected non-radiative recombination losses as a function of $\Delta E_{S_1,CT}$ and $V_{oc,rad}$, respectively, for the cases of no mixing ($V_{S_1,CT} = 0$, i.e. no mixing), small electronic coupling (small $V_{S_1,CT}$) and high electronic coupling (large $V_{S_1,CT}$) between CT state and first excited singlet state, using the parameters in Table S12.

In the case of no mixing, the $\Delta V_{oc,nrad}$ ($\Delta E_{S_1,CT}$) dependence is fairly linear for all energetic offsets due to the constancy in $f_{S_0,CT}$. When plotted against V_{rad} there is a slightly superlinear decrease in $\Delta V_{oc,nrad}$ at high $V_{oc,rad}$ values. Hence, assuming no mixing between CT and S_1 states is sufficient to explain the behaviour of large $\Delta E_{S_1,CT}$ systems, such as in the case of IT-4F, where hybridization is insufficient to amplify $f^*_{S_0,CT}$ (i.e. EL intensity). For cases with low $\Delta E_{S_1,CT}$, however, clearly the hybridization of CT and singlet states must be taken into account in order to explain the strong decrease in $\Delta V_{oc,nrad}$ observed in the experimental results (e.g. C8-ITIC plotted in Figure 5c and d); even for a low CT to S_1 electronic coupling, a strong reduction in $\Delta V_{oc,nrad}$ is observed as E_{CT} approaches E_{S_1} compared to the two-state model, and in the event of strong coupling there is a strong reduction in $\Delta V_{oc,nrad}$ across a large range of $\Delta E_{S_1,CT}$ (Figure 5c). Similarly, if we examine the plot of $\Delta V_{oc,nrad}(V_{oc,rad})$ (Figure 5d), we can see that at low electronic coupling $\Delta V_{oc,nrad}$ is decreased compared to the case of no mixing, whilst with strong coupling $\Delta V_{oc,nrad}$ is strongly decreased at all $V_{oc,rad}$. From these results, we suggest that there is a threshold that must be reached in terms of hybridization of the energy levels for there to be a significant impact on $\Delta V_{oc,nrad}$ which arises due to a stronger dependency of $\Delta V_{oc,nrad}$ on E_{CT} than on $f^*_{S_0,CT}$.

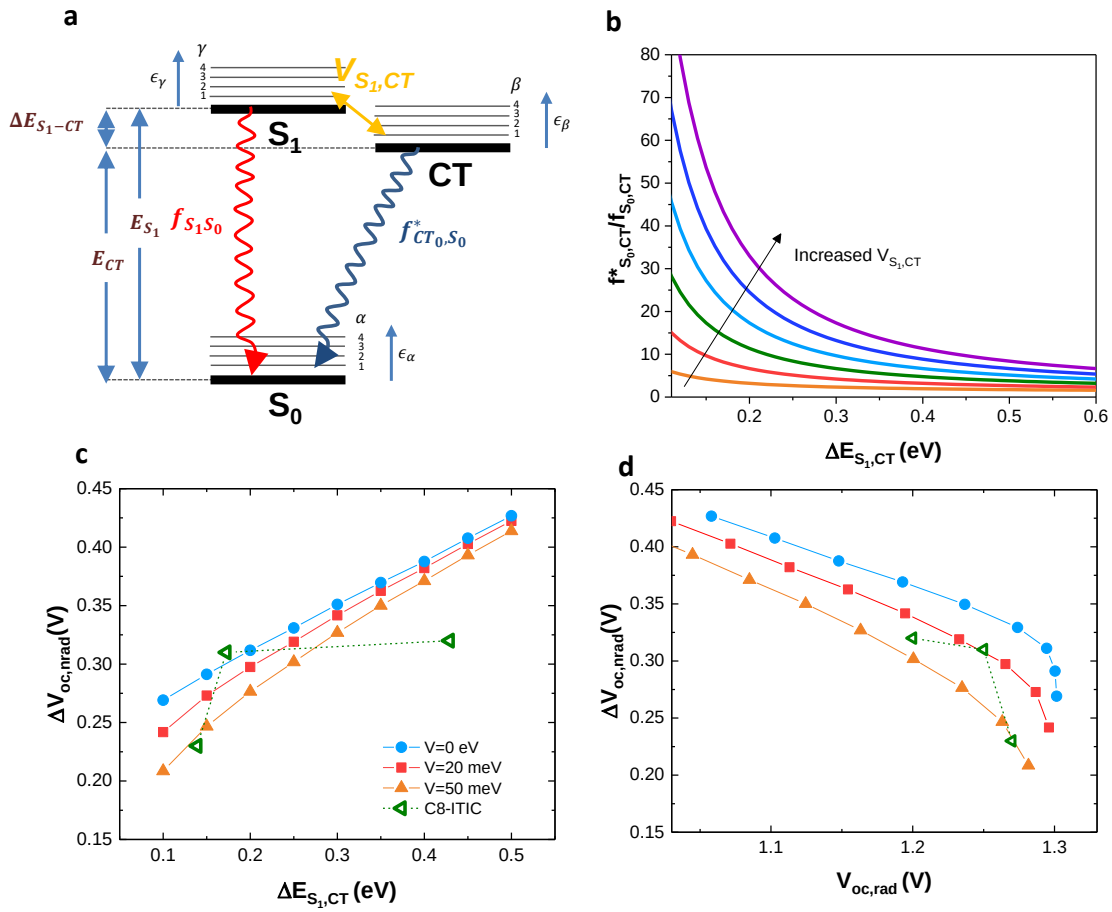

Figure 5: **Simulated oscillator strengths and non-radiative voltage losses** a) Schematic of the three-state model, $V_{S_1,CT}$is the coupling between the lowest exciton state and the CT state, and E_{S1}, E_{CT} the energies of the first excited singlet state S_1 and the CT state, respectively. $\epsilon_\alpha, \epsilon_\beta, \epsilon_\gamma$ the energies of the vibrational states of the 3 states the ground state S_0, S_1 and CT, respectively .b)The simulated effect CT-ground state oscillator strength f^*_{CT,S_0} as a function of driving energy $\Delta E_{S_1,CT}$, for different $S_1 \rightarrow$ CT state coupling energies ranging from 10 (orange) to 60 (purple) meV, an oscillator strength in the absence of any coupling of 0.02, and $f_{S_1,S_0} = 5$. The inset in a) shows a schematic of the three state model used to obtain f^*_{CT,S_0}. c) and d) show the simulated non-radiative voltage loss $\Delta V_{oc,nrad}$ as a function of $\Delta E_{S_1,CT}$ and $V_{oc,rad}$, respectively, for the cases of no electronic coupling (V=0 eV), low electronic coupling (V=20 meV) and medium electronic coupling (V=50 meV) between the CT and first excited singlet state. The experimental results for C8-ITIC are also plotted (green) in c) and d).

Dependence of Non-Radiative Voltage Loss on Luminescence of Pristine Materials

It has recently been observed that a high photoluminescence quantum efficiency (PLQE) of the pristine materials in a D-A blend is correlated to reduced voltage losses in BHJ solar cells.[38] This may help to explain why many solar cells based on luminescent acceptors exhibit lower voltage losses than those based on fullerenes. From our own results we cannot conclude that there is a large inherent difference in the energy loss behaviour between non-fullerene and

fullerene acceptors at low $\Delta E_{S_1,CT}$, since a similarly large reduction in $\Delta V_{oc,nrad}$ can be achieved with D-4F:(21,40)bis[60]PCBM as with D-4F:ITIC and D-4F:C8-ITIC. However, we remark that the absolute $\Delta V_{oc,nrad}$ are much larger with (21,40)bis[60]PCBM blends than with C8-ITIC and ITIC. This may be due to the lower radiative efficiency of the lowest band gap material in the blend with (21,40)bis[60]PCBM (the donor) than with C8-ITIC or ITIC (the acceptor), that is to say f_{S_1,S_0} is smaller for the (21,40)bis[60]PCBM, leading to higher $\Delta V_{oc,nrad}$ values, which agrees with the aforementioned recent findings[38]. However, since f_{S_1,S_0} appears only as a linear term in $f^*_{S_0,CT}$ at low $\Delta E_{S_1,CT}$, whilst $\Delta E_{S_1,CT}$ and $V_{S_1,CT}$ appear as quadratic terms, this low radiative ability of the first excited state does not prevent a strong reduction in $\Delta V_{oc,nrad}$ at low $\Delta E_{S_1,CT}$. In order for fullerene-based blends to achieve similarly low $\Delta V_{oc,nrad}$ as non-fullerene-based cells, lowband gap donors with high f_{S_1,S_0} should hence be used.

Effect of Hybridization on Device Performance

Finally, we comment on the relationship between hybridization and device performance, bearing in mind the crucial question in organic photovoltaics of whether it is possible to simultaneously achieve low voltage losses, and high fill factor and EQE. First, we have established that the hybridisation of the CT state and the excited singlet state significantly increases the luminescence of the lowest CT state, which reduces the non-radiative voltage losses. However, the increase of the CT state luminescence also reduces $V_{oc,rad}$, which increases the voltage losses due to broadening of the absorption edge ($\Delta V_{oc,abs}$).[37] Since $V_{oc} = V_{oc,rad} - \Delta V_{oc,nrad}$, the mixing of the CT and S_1 states is therefore not always beneficial to the V_{oc} of the device; instead our model predicts that the highest gain in V_{oc} is achieved for high $V_{S_1,CT}$ values at low $\Delta E_{S_1,CT}$ (Figure S13). Second, we first note from our experimental results that while efficient charge generation can still occur in some of the very low offset blends (EQE over 70% for D-4F:C8-ITIC), the best device performances are realised at intermediate offsets with D-2F, due to both their superior J_{sc} and FF, with non-radiative voltage losses of around 300 mV for D-2F:ITIC and D-2F:C8-ITIC. While this may be partially, or fully, attributable to morphological effects, it begs the question of whether complete hybridization of the CT and S_1 states can still yield efficient charge generation under some circumstances.

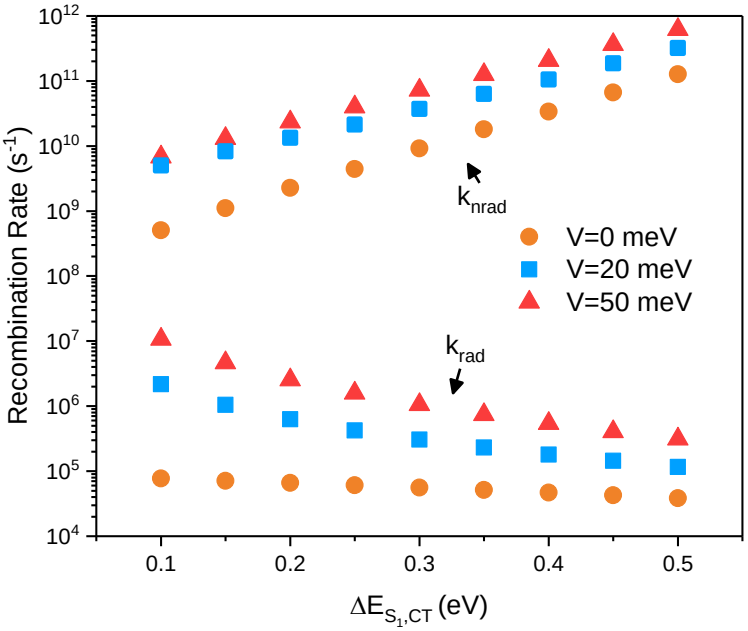

Figure 6: **Recombination rates as a function of driving energy.** The simulated radiative and non-radiative recombination rates are plotted for the cases of no, low and medium coupling between CT and first excited singlet states as a function of driving energy.

It has recently been shown that in low $\Delta E_{S_1,CT}$ systems singlet exciton quenching occurs at a much slower rate than in high $\Delta E_{S_1,CT}$ systems.[36] In Figure 6 we plot the calculated non-radiative and radiative recombination rates which led to the $\Delta V_{oc,nrad}$ values in Figure 5c via equation S5, against $\Delta E_{S_1,CT}$. Firstly, we note that in the absence of hybridization ($V = 0$ meV), the non-radiative recombination rate decreases with decreasing $\Delta E_{S_1,CT}$, whilst the radiative recombination rates stays roughly constant. Because $\Delta V_{oc,nrad}$ varies with the logarithm of the ratio of total to radiative recombination rates, this leads to the observed decrease of $\Delta V_{oc,nrad}$ with decreasing $\Delta E_{S_1,CT}$.[35] Secondly, we note that when hybridization is taken into account, the non-radiative and radiative recombination rates both increase over the $V = 0$ case, with both rates being about an order of magnitude larger at low $\Delta E_{S_1,CT}$ even with low coupling ($V = 0.02$ meV), due to the increase in the oscillator strength of the $CT \rightarrow S_0$ transition. The reason why $\Delta V_{oc,nrad}$ is decreased is because k_{rad} increases more than k_{nrad}, which is also why a larger electronic coupling decreases $\Delta V_{oc,nrad}$, since the larger coupling has little effect on k_{nrad}, but continues to increase k_{rad}.

The total recombination rate (Figure S14), which depends primarily on k_{nrad}, is then around an order of magnitude lower in the uncoupled case than in the coupled case. This picture of increased recombination rate may be part of the explanation as to why the blends in our study with very low $\Delta V_{oc,nrad}$ values (D-4F:ITIC and D-4F:C8-ITIC), have lower FF and EQE values than blends with higher $\Delta V_{oc,nrad}$ values. A complete picture on charge generation, of course, has to inv olve both the effects of morphology, and the presence and influence of the charge-separated state, and is beyond the scope of this work. [67-78]

Conclusions

We have presented a systematic study of the role that hybridization between charge transfer states and the first excited singlet, or local exciton, state plays in determining the voltage loss due to non-radiative recombination in organic solar cells. By measuring the electroluminescence spectrum and sub-band gap EQE of a large number of donor:acceptor combinations with a broad spectrum of driving energies $\Delta E_{S_1,CT}$, we have shown that below a certain $\Delta E_{S_1,CT}$, which is material dependent, CT and S_1 become progressively more hybridized with decreasing $\Delta E_{S_1,CT}$, to a point where the absorption and emission from the CT state is spectrally indistinguishable from that of the first excited singlet state. When $\Delta E_{S_1,CT}$ is sufficiently small, state hybridization leads to a large increase in the luminescence of the CT state, and a corresponding large decrease in the non-radiative recombination voltage losses.

By combining a three-state model incorporating the effects of wavefunction overlap between singlet and CT states, with a model of non-radiative recombination, we show this drop in $\Delta V_{oc,nrad}$ at low $\Delta E_{S_1,CT}$ can be explained by an increase in the oscillator strength of the CT to ground state transition due to the interaction between the CT state and first excited singlet state wavefunctions. We find that $\Delta V_{oc,nrad}$ can be reduced further by designing systems with strong electronic coupling between CT and first excited states in addition to having strongly luminescent first excited to ground state transitions. For example, for material combinations with a relatively high electronic coupling of 100 meV together with a relatively luminescent low gap component ($f_{S_1,S_0} \approx 5$), $\Delta V_{oc,nrad}$ values approaching 0.17V are in reach. Finally, we show that whilst the non-radiative recombination voltage losses may be reduced in systems with low $\Delta E_{S_1,CT}$, the total recombination rate is increased, which may put a limit on how far voltage losses can be reduced in organic solar cells without affecting the total device performance.

Acknowledgements

FE and MA thank the Engineering and Physical Sciences Research Council (EPSRC) for support via doctoral studentships. JN is grateful for funding from the EPSRC (grants EP/ P005543/1 and EP/M025020/1) and the European Research Council (ERC) under the European Union's Horizon 2020 research and innovation program (grant agreement No 742708). FE, MA and JN thank Artem Bakulin, Nathaniel Gallop, Shawn Zheng and Thomas Kirchartz for helpful discussions.

Supporting Information Available:

Energy levels of the materials, results from DFT calculations, full device performance parameters, AFM scans, plots of V_{oc} and $V_{oc,rad}$ against driving force, PL spectra of pristine materials, full sub-band gap EQE and EL spectra for all blends, injection dependent EL spectra, full EQE spectra, PL quenching spectra of blends, examples of fits to EL results, examples of EL fits to EQE to extract voltage losses, full voltage loss results table, recombination rates simulation results, simulated V_{oc} as a function of $\Delta E_{S_1,CT}$.

This material is available free of charge via the Internet at http://pubs.acs.org

References

1. Li, W.; Ye, L.; Li, S.; Yao, H.; Ade, H.; Hou, J., A High-Efficiency Organic Solar Cell Enabled by the Strong Intramolecular Electron Push–Pull Effect of the Nonfullerene Acceptor. *Advanced Materials* **2018,** *30*, 1707170.
2. Zheng, Z.; Hu, Q.; Zhang, S.; Zhang, D.; Wang, J.; Xie, S.; Wang, R.; Qin, Y.; Li, W.; Hong, L.; Liang, N.; Liu, F.; Zhang, Y.; Wei, Z.; Tang, Z.; Russell, T. P.; Hou, J.; Zhou, H., A Highly Efficient Non-Fullerene Organic Solar Cell with a Fill Factor over 0.80 Enabled by a Fine-Tuned Hole-Transporting Layer. *Advanced Materials* **2018,** *30*, 1801801.
3. Zhang, H.; Yao, H.; Hou, J.; Zhu, J.; Zhang, J.; Li, W.; Yu, R.; Gao, B.; Zhang, S.; Hou, J., Over 14% Efficiency in Organic Solar Cells Enabled by Chlorinated Nonfullerene Small-Molecule Acceptors. *Advanced Materials* **2018,** *0*, 1800613.
4. Zhao, W.; Li, S.; Yao, H.; Zhang, S.; Zhang, Y.; Yang, B.; Hou, J., Molecular Optimization Enables over 13% Efficiency in Organic Solar Cells. *Journal of the American Chemical Society* **2017,** *139*, 7148-7151.
5. Fei, Z.; Eisner, F. D.; Jiao, X.; Azzouzi, M.; Röhr, J. A.; Han, Y.; Shahid, M.; Chesman, A. S. R.; Easton, C. D.; McNeill, C. R.; Anthopoulos, T. D.; Nelson, J.; Heeney, M., An Alkylated Indacenodithieno[3,2-B]Thiophene-Based Nonfullerene Acceptor with High Crystallinity Exhibiting Single Junction Solar Cell Efficiencies Greater Than 13% with Low Voltage Losses. *Advanced Materials 30*, 1705209.
6. Yuan, J.; Zhang, Y.; Zhou, L.; Zhang, G.; Yip, H.-L.; Lau, T.-K.; Lu, X.; Zhu, C.; Peng, H.; Johnson, P. A.; Leclerc, M.; Cao, Y.; Ulanski, J.; Li, Y.; Zou, Y., Single-Junction Organic Solar Cell with over 15% Efficiency Using Fused-Ring Acceptor with Electron-Deficient Core. *Joule* **2019,** *3*, 1-12.
7. Meng, L.; Zhang, Y.; Wan, X.; Li, C.; Zhang, X.; Wang, Y.; Ke, X.; Xiao, Z.; Ding, L.; Xia, R.; Yip, H.-L.; Cao, Y.; Chen, Y., Organic and Solution-Processed Tandem Solar Cells with 17.3% Efficiency. *Science* **2018,** *361*, 1094-1098.

8. Hou, J.; Inganäs, O.; Friend, R. H.; Gao, F., Organic Solar Cells Based on Non-Fullerene Acceptors. *Nature Materials* **2018,** *17*, 119.
9. Chen, S.; Wang, Y.; Zhang, L.; Zhao, J.; Chen, Y.; Zhu, D.; Yao, H.; Zhang, G.; Ma, W.; Friend, R. H.; Chow, P. C. Y.; Gao, F.; Yan, H., Efficient Nonfullerene Organic Solar Cells with Small Driving Forces for Both Hole and Electron Transfer. *Advanced Materials* **2018,** *0*, 1804215.
10. Liu, J.; Chen, S.; Qian, D.; Gautam, B.; Yang, G.; Zhao, J.; Bergqvist, J.; Zhang, F.; Ma, W.; Ade, H.; Inganäs, O.; Gundogdu, K.; Gao, F.; Yan, H., Fast Charge Separation in a Non-Fullerene Organic Solar Cell with a Small Driving Force. *Nature Energy* **2016,** *1*, 16089.
11. Mihailetchi, V. D.; Koster, L. J. A.; Hummelen, J. C.; Blom, P. W. M., Photocurrent Generation in Polymer-Fullerene Bulk Heterojunctions. *Physical Review Letters* **2004,** *93*, 216601.
12. Limpinsel, M.; Wagenpfahl, A.; Mingebach, M.; Deibel, C.; Dyakonov, V., Photocurrent in Bulk Heterojunction Solar Cells. *Physical Review B* **2010,** *81*, 085203.
13. Peumans, P.; Forrest, S. R., Separation of Geminate Charge-Pairs at Donor–Acceptor Interfaces in Disordered Solids. *Chemical Physics Letters* **2004,** *398*, 27-31.
14. Faist, M. A.; Kirchartz, T.; Gong, W.; Ashraf, R. S.; McCulloch, I.; de Mello, J. C.; Ekins-Daukes, N. J.; Bradley, D. D. C.; Nelson, J., Competition between the Charge Transfer State and the Singlet States of Donor or Acceptor Limiting the Efficiency in Polymer:Fullerene Solar Cells. *Journal of the American Chemical Society* **2012,** *134*, 685-692.
15. Tvingstedt, K.; Vandewal, K.; Gadisa, A.; Zhang, F.; Manca, J.; Inganäs, O., Electroluminescence from Charge Transfer States in Polymer Solar Cells. *Journal of the American Chemical Society* **2009,** *131*, 11819-11824.
16. Benson-Smith, J. J.; Goris, L.; Vandewal, K.; Haenen, K.; Manca, J. V.; Vanderzande, D.; Bradley, D. D. C.; Nelson, J., Formation of a Ground-State Charge-Transfer Complex in Polyfluorene//[6,6]-Phenyl-C61 Butyric Acid Methyl Ester (Pcbm) Blend Films and Its Role in the Function of Polymer/Pcbm Solar Cells. *Advanced Functional Materials* **2007,** *17*, 451-457.
17. Janssen, R. A. J.; Nelson, J., Factors Limiting Device Efficiency in Organic Photovoltaics. *Advanced Materials* **2012,** *25*, 1847-1858.
18. Scharber, M. C.; Mühlbacher, D.; Koppe, M.; Denk, P.; Waldauf, C.; Heeger, A. J.; Brabec, C. J., Design Rules for Donors in Bulk-Heterojunction Solar Cells—Towards 10 % Energy-Conversion Efficiency. *Advanced Materials* **2006,** *18*, 789-794.
19. Vandewal, K.; Ma, Z.; Bergqvist, J.; Tang, Z.; Wang, E.; Henriksson, P.; Tvingstedt, K.; Andersson, M. R.; Zhang, F.; Inganäs, O., Quantification of Quantum Efficiency and Energy Losses in Low Bandgap Polymer:Fullerene Solar Cells with High Open-Circuit Voltage. *Advanced Functional Materials* **2012,** *22*, 3480-3490.
20. Kawashima, K.; Tamai, Y.; Ohkita, H.; Osaka, I.; Takimiya, K., High-Efficiency Polymer Solar Cells with Small Photon Energy Loss. *Nature Communications* **2015,** *6*, 10085.
21. Wang, E.; Ma, Z.; Zhang, Z.; Vandewal, K.; Henriksson, P.; Inganäs, O.; Zhang, F.; Andersson, M. R., An Easily Accessible Isoindigo-Based Polymer for High-Performance Polymer Solar Cells. *Journal of the American Chemical Society* **2011,** *133*, 14244-14247.
22. Yang, D.; Wang, Y.; Sano, T.; Gao, F.; Sasabe, H.; Kido, J., A Minimal Non-Radiative Recombination Loss for Efficient Non-Fullerene All-Small-Molecule Organic Solar Cells with a Low Energy Loss of 0.54 ev and High Open-Circuit Voltage of 1.15 V. *Journal of Materials Chemistry A* **2018,** *6*, 13918-13924.
23. Chen, S.; Liu, Y.; Zhang, L.; Chow, P. C. Y.; Wang, Z.; Zhang, G.; Ma, W.; Yan, H., A Wide-Bandgap Donor Polymer for Highly Efficient Non-Fullerene Organic Solar Cells with a Small Voltage Loss. *Journal of the American Chemical Society* **2017,** *139*, 6298-6301.
24. Baran, D.; Kirchartz, T.; Wheeler, S.; Dimitrov, S.; Abdelsamie, M.; Gorman, J.; Ashraf, R. S.; Holliday, S.; Wadsworth, A.; Gasparini, N.; Kaienburg, P.; Yan, H.; Amassian, A.; Brabec, C. J.; Durrant, J. R.; McCulloch, I., Reduced Voltage Losses Yield 10% Efficient Fullerene Free Organic Solar Cells with >1 V Open Circuit Voltages. *Energy & Environmental Science* **2016,** *9*, 3783-3793.

25. Sun, C.; Pan, F.; Bin, H.; Zhang, J.; Xue, L.; Qiu, B.; Wei, Z.; Zhang, Z.-G.; Li, Y., A Low Cost and High Performance Polymer Donor Material for Polymer Solar Cells. *Nature Communications* **2018,** *9*, 743.
26. Fu, H.; Wang, Y.; Meng, D.; Ma, Z.; Li, Y.; Gao, F.; Wang, Z.; Sun, Y., Suppression of Recombination Energy Losses by Decreasing the Energetic Offsets in Perylene Diimide-Based Nonfullerene Organic Solar Cells. *ACS Energy Letters* **2018**, 2729-2735.
27. Vandewal, K.; Tvingstedt, K.; Gadisa, A.; Inganäs, O.; Manca, J. V., Relating the Open-Circuit Voltage to Interface Molecular Properties of Donor:Acceptor Bulk Heterojunction Solar Cells. *Physical Review B* **2010,** *81*, 125204.
28. Bartesaghi, D.; Pérez, I. d. C.; Kniepert, J.; Roland, S.; Turbiez, M.; Neher, D.; Koster, L. J. A., Competition between Recombination and Extraction of Free Charges Determines the Fill Factor of Organic Solar Cells. *Nature Communications* **2015,** *6*, 7083.
29. Burke, T. M.; Sweetnam, S.; Vandewal, K.; McGehee, M. D., Beyond Langevin Recombination: How Equilibrium between Free Carriers and Charge Transfer States Determines the Open-Circuit Voltage of Organic Solar Cells. *Advanced Energy Materials* **2015,** *5*, 1500123.
30. Vaynzof, Y.; Bakulin, A. A.; Gélinas, S.; Friend, R. H., Direct Observation of Photoinduced Bound Charge-Pair States at an Organic-Inorganic Semiconductor Interface. *Physical Review Letters* **2012,** *108*, 246605.
31. Sulas, D. B.; Yao, K.; Intemann, J. J.; Williams, S. T.; Li, C.-Z.; Chueh, C.-C.; Richards, J. J.; Xi, Y.; Pozzo, L. D.; Schlenker, C. W.; Jen, A. K. Y.; Ginger, D. S., Open-Circuit Voltage Losses in Selenium-Substituted Organic Photovoltaic Devices from Increased Density of Charge-Transfer States. *Chemistry of Materials* **2015,** *27*, 6583-6591.
32. Vandewal, K.; Tvingstedt, K.; Inganäs, O., Polarization Anisotropy of Charge Transfer Absorption and Emission of Aligned Polymer:Fullerene Blend Films. *Physical Review B* **2012,** *86*, 035212.
33. Koster, L. J. A.; Shaheen, S. E.; Hummelen, J. C., Pathways to a New Efficiency Regime for Organic Solar Cells. *Advanced Energy Materials* **2012,** *2*, 1246-1253.
34. Yao, J.; Kirchartz, T.; Vezie, M. S.; Faist, M. A.; Gong, W.; He, Z.; Wu, H.; Troughton, J.; Watson, T.; Bryant, D.; Nelson, J., Quantifying Losses in Open-Circuit Voltage in Solution-Processable Solar Cells. *Physical Review Applied* **2015,** *4*, 014020.
35. Benduhn, J.; Tvingstedt, K.; Piersimoni, F.; Ullbrich, S.; Fan, Y.; Tropiano, M.; McGarry, K. A.; Zeika, O.; Riede, M. K.; Douglas, C. J.; Barlow, S.; Marder, S. R.; Neher, D.; Spoltore, D.; Vandewal, K., Intrinsic Non-Radiative Voltage Losses in Fullerene-Based Organic Solar Cells. *Nature Energy* **2017,** *2*, 17053.
36. Qian, D.; Zheng, Z.; Yao, H.; Tress, W.; Hopper, T. R.; Chen, S.; Li, S.; Liu, J.; Chen, S.; Zhang, J.; Liu, X.-K.; Gao, B.; Ouyang, L.; Jin, Y.; Pozina, G.; Buyanova, I. A.; Chen, W. M.; Inganäs, O.; Coropceanu, V.; Bredas, J.-L.; Yan, H.; Hou, J.; Zhang, F.; Bakulin, A. A.; Gao, F., Design Rules for Minimizing Voltage Losses in High-Efficiency Organic Solar Cells. *Nature Materials* **2018,** *17*, 703-709.
37. Azzouzi, M.; Yan, J.; Kirchartz, T.; Liu, K.; Wang, J.; Wu, H.; Nelson, J., Non-Radiative Energy Losses in Bulk-Heterojunction Organic Photovoltaics. *Physical Review X* **2018,** *8*, 031055.
38. Ziffer, M. E.; Jo, S. B.; Zhong, H.; Ye, L.; Liu, H.; Lin, F.; Zhang, J.; Li, X.; Ade, H. W.; Jen, A. K. Y.; Ginger, D. S., Long-Lived, Non-Geminate, Radiative Recombination of Photogenerated Charges in a Polymer/Small-Molecule Acceptor Photovoltaic Blend. *Journal of the American Chemical Society* **2018,** *140*, 9996-10008.
39. Pasman, P.; Rob, F.; Verhoeven, J. W., Intramolecular Charge-Transfer Absorption and Emission Resulting from through-Bond Interaction in Bichromophoric Molecules. *Journal of the American Chemical Society* **1982,** *104*, 5127-5133.
40. Bixon, M.; Jortner, J.; Verhoeven, J. W., Lifetimes for Radiative Charge Recombination in Donor-Acceptor Molecules. *Journal of the American Chemical Society* **1994,** *116*, 7349-7355.

41. Joseph, S.; Ravva, M. K.; Bredas, J.-L., Charge-Transfer Dynamics in the Lowest Excited State of a Pentacene–Fullerene Complex: Implications for Organic Solar Cells. *The Journal of Physical Chemistry Letters* **2017,** *8*, 5171-5176.
42. D'Avino, G.; Muccioli, L.; Olivier, Y.; Beljonne, D., Charge Separation and Recombination at Polymer–Fullerene Heterojunctions: Delocalization and Hybridization Effects. *The Journal of Physical Chemistry Letters* **2016,** *7*, 536-540.
43. Few, S.; Frost, J. M.; Kirkpatrick, J.; Nelson, J., Influence of Chemical Structure on the Charge Transfer State Spectrum of a Polymer:Fullerene Complex. *The Journal of Physical Chemistry C* **2014,** *118*, 8253-8261.
44. Liu, Y.; Zuo, L.; Shi, X.; Jen, A. K. Y.; Ginger, D. S., Unexpectedly Slow yet Efficient Picosecond to Nanosecond Photoinduced Hole-Transfer Occurs in a Polymer/Nonfullerene Acceptor Organic Photovoltaic Blend. *ACS Energy Letters* **2018**, 2396-2403.
45. Qian, D.; Ye, L.; Zhang, M.; Liang, Y.; Li, L.; Huang, Y.; Guo, X.; Zhang, S.; Tan, Z. a.; Hou, J., Design, Application, and Morphology Study of a New Photovoltaic Polymer with Strong Aggregation in Solution State. *Macromolecules* **2012,** *45*, 9611-9617.
46. Zhao, W.; Qian, D.; Zhang, S.; Li, S.; Inganäs, O.; Gao, F.; Hou, J., Fullerene-Free Polymer Solar Cells with over 11% Efficiency and Excellent Thermal Stability. *Advanced Materials* **2016,** *28*, 4734-4739.
47. Lin, Y.; Wang, J.; Zhang, Z.-G.; Bai, H.; Li, Y.; Zhu, D.; Zhan, X., An Electron Acceptor Challenging Fullerenes for Efficient Polymer Solar Cells. *Advanced Materials* **2015,** *27*, 1170-1174.
48. Mendaza, A. D.; Melianas, A.; Rossbauer, S.; Backe, O.; Nordstierna, L.; Erhart, P.; Olsson, E.; Anthopoulos, T. D.; Inganas, O.; Muller, C., High-Entropy Mixtures of Pristine Fullerenes for Solution-Processed Transistors and Solar Cells. *Adv Mater* **2015,** *27*, 7325-31.
49. Liu, T.; Abrahams, I.; Dennis, T. J. S., Structural Identification of 19 Purified Isomers of the Opv Acceptor Material Bispcbm by 13c Nmr and Uv–Vis Absorption Spectroscopy and High-Performance Liquid Chromatography. *The Journal of Physical Chemistry A* **2018,** *122*, 4138-4152.
50. Shi, W.; Hou, X.; Liu, T.; Zhao, X.; Sieval, A. B.; Hummelen, J. C.; Dennis, T. J. S., Purification and Electronic Characterisation of 18 Isomers of the Opv Acceptor Material Bis-[60]Pcbm. *Chemical Communications* **2017,** *53*, 975-978.
51. Faist, M. A.; Shoaee, S.; Tuladhar, S.; Dibb, G. F. A.; Foster, S.; Gong, W.; Kirchartz, T.; Bradley, D. D. C.; Durrant, J. R.; Nelson, J., Understanding the Reduced Efficiencies of Organic Solar Cells Employing Fullerene Multiadducts as Acceptors. *Advanced Energy Materials* **2013,** *3*, 744-752.
52. Kranthiraja, K.; Kim, S.; Lee, C.; Gunasekar, K.; Sree Vijaya, G.; Gautam, B.; Gundogdu, K.; Jin, S.-H.; Kim Bumjoon, J., The Impact of Sequential Fluorination of Π-Conjugated Polymers on Charge Generation in All-Polymer Solar Cells. *Advanced Functional Materials* **2017,** *27*, 1701256.
53. Yin, J.; Chaitanya, K.; Ju, X.-H., Theoretical Study of the Fluorination Effect on Charge Transport Properties in Fused Thiophene Derivatives. *RSC Advances* **2015,** *5*, 65192-65202.
54. Shin, J.; Kim, M.; Lee, J.; Kim, H. G.; Hwang, H.; Cho, K., Positional Effects of Fluorination in Conjugated Side Chains on Photovoltaic Properties of Donor–Acceptor Copolymers. *Chemical Communications* **2017,** *53*, 1176-1179.
55. Zhang, Q.; Kelly, M. A.; Bauer, N.; You, W., The Curious Case of Fluorination of Conjugated Polymers for Solar Cells. *Accounts of Chemical Research* **2017,** *50*, 2401-2409.
56. Son, H. J.; Wang, W.; Xu, T.; Liang, Y.; Wu, Y.; Li, G.; Yu, L., Synthesis of Fluorinated Polythienothiophene-Co-Benzodithiophenes and Effect of Fluorination on the Photovoltaic Properties. *Journal of the American Chemical Society* **2011,** *133*, 1885-1894.
57. Ko, S.-J.; Hoang, Q. V.; Song, C. E.; Uddin, M. A.; Lim, E.; Park, S. Y.; Lee, B. H.; Song, S.; Moon, S.-J.; Hwang, S.; Morin, P.-O.; Leclerc, M.; Su, G. M.; Chabinyc, M. L.; Woo, H. Y.; Shin, W. S.; Kim, J. Y., High-Efficiency Photovoltaic Cells with Wide Optical Band Gap Polymers Based on Fluorinated Phenylene-Alkoxybenzothiadiazole. *Energy & Environmental Science* **2017,** *10*, 1443-1455.
58. Vandewal, K.; Benduhn, J.; Nikolis, V. C., How to Determine Optical Gaps and Voltage Losses in Organic Photovoltaic Materials. *Sustainable Energy & Fuels* **2018,** *2*, 538-544.

59. Kahle, F.-J.; Rudnick, A.; Bässler, H.; Köhler, A., How to Interpret Absorption and Fluorescence Spectra of Charge Transfer States in an Organic Solar Cell. *Materials Horizons* **2018,** *5*, 837-848.
60. Vandewal, K.; Benduhn, J.; Schellhammer, K. S.; Vangerven, T.; Rückert, J. E.; Piersimoni, F.; Scholz, R.; Zeika, O.; Fan, Y.; Barlow, S.; Neher, D.; Marder, S. R.; Manca, J.; Spoltore, D.; Cuniberti, G.; Ortmann, F., Absorption Tails of Donor:C60 Blends Provide Insight into Thermally Activated Charge-Transfer Processes and Polaron Relaxation. *Journal of the American Chemical Society* **2017,** *139*, 1699-1704.
61. Jortner, J., Temperature Dependent Activation Energy for Electron Transfer between Biological Molecules. *The Journal of Chemical Physics* **1976,** *64*, 4860-4867.
62. Arndt, A. P.; Gerhard, M.; Koch, M.; Lemmer, U.; Howard, I. A., Identifying Charge-Transfer States in Polymer:Fullerene Heterojunctions by Their Emission Polarization Anisotropy. *The Journal of Physical Chemistry C* **2017,** *121*, 6357-6364.
63. Huang, Y.-s.; Westenhoff, S.; Avilov, I.; Sreearunothai, P.; Hodgkiss, J. M.; Deleener, C.; Friend, R. H.; Beljonne, D., Electronic Structures of Interfacial States Formed at Polymeric Semiconductor Heterojunctions. *Nature Materials* **2008,** *7*, 483.
64. Benduhn, J.; Piersimoni, F.; Londi, G.; Kirch, A.; Widmer, J.; Koerner, C.; Beljonne, D.; Neher, D.; Spoltore, D.; Vandewal, K., Impact of Triplet Excited States on the Open-Circuit Voltage of Organic Solar Cells. *Advanced Energy Materials* **2018,** *8*, 1800451.
65. Kurpiers, J.; Ferron, T.; Roland, S.; Jakoby, M.; Thiede, T.; Jaiser, F.; Albrecht, S.; Janietz, S.; Collins, B. A.; Howard, I. A.; Neher, D., Probing the Pathways of Free Charge Generation in Organic Bulk Heterojunction Solar Cells. *Nature Communications* **2018,** *9*, 2038.
66. Rust, M.; Lappe, J.; Cave, R. J., Multistate Effects in Calculations of the Electronic Coupling Element for Electron Transfer Using the Generalized Mulliken−Hush Method. *The Journal of Physical Chemistry A* **2002,** *106*, 3930-3940.
67. Sini, G.; Schubert, M.; Risko, C.; Roland, S.; Lee, O. P.; Chen, Z.; Richter, T. V.; Dolfen, D.; Coropceanu, V.; Ludwigs, S.; Scherf, U.; Facchetti, A.; Fréchet, J. M. J.; Neher, D., On the Molecular Origin of Charge Separation at the Donor–Acceptor Interface. *Advanced Energy Materials* **2018,** *8*, 1702232.
68. Collado-Fregoso, E.; Pugliese, S. N.; Wojcik, M.; Benduhn, J.; Bar-Or, E.; Perdigon Toro, L.; Hörmann, U.; Spoltore, D.; Vandewal, K.; Hodgkiss, J. M.; Neher, D., An Energy-Gap Law for Photocurrent Generation in Fullerene-Based Organic Solar Cells – the Case of Low-Donor Content-Blends. *Journal of the American Chemical Society* **2019**.
69. Ran, N. A.; Roland, S.; Love, J. A.; Savikhin, V.; Takacs, C. J.; Fu, Y.-T.; Li, H.; Coropceanu, V.; Liu, X.; Brédas, J.-L.; Bazan, G. C.; Toney, M. F.; Neher, D.; Nguyen, T.-Q., Impact of Interfacial Molecular Orientation on Radiative Recombination and Charge Generation Efficiency. *Nature Communications* **2017,** *8*, 79.
70. Menke, S. M.; Cheminal, A.; Conaghan, P.; Ran, N. A.; Greehnam, N. C.; Bazan, G. C.; Nguyen, T.-Q.; Rao, A.; Friend, R. H., Order Enables Efficient Electron-Hole Separation at an Organic Heterojunction with a Small Energy Loss. *Nature Communications* **2018,** *9*, 277.
71. Devižis, A.; De Jonghe-Risse, J.; Hany, R.; Nüesch, F.; Jenatsch, S.; Gulbinas, V.; Moser, J.-E., Dissociation of Charge Transfer States and Carrier Separation in Bilayer Organic Solar Cells: A Time-Resolved Electroabsorption Spectroscopy Study. *Journal of the American Chemical Society* **2015,** *137*, 8192-8198.
72. Gallaher, J. K.; Prasad, S. K. K.; Uddin, M. A.; Kim, T.; Kim, J. Y.; Woo, H. Y.; Hodgkiss, J. M., Spectroscopically Tracking Charge Separation in Polymer : Fullerene Blends with a Three-Phase Morphology. *Energy & Environmental Science* **2015,** *8*, 2713-2724.
73. Gerhard, M.; Arndt, A. P.; Bilal, M.; Lemmer, U.; Koch, M.; Howard, I. A., Field-Induced Exciton Dissociation in Ptb7-Based Organic Solar Cells. *Physical Review B* **2017,** *95*, 195301.

74. Chen, X.-K.; Ravva Mahesh, K.; Li, H.; Ryno Sean, M.; Brédas, J.-L., Effect of Molecular Packing and Charge Delocalization on the Nonradiative Recombination of Charge-Transfer States in Organic Solar Cells. *Advanced Energy Materials* **2016,** *6*, 1601325.
75. Kahle, F.-J.; Saller, C.; Olthof, S.; Li, C.; Lebert, J.; Weiß, S.; Herzig, E. M.; Hüttner, S.; Meerholz, K.; Strohriegl, P.; Köhler, A., Does Electron Delocalization Influence Charge Separation at Donor–Acceptor Interfaces in Organic Photovoltaic Cells? *The Journal of Physical Chemistry C* **2018,** *122*, 21792-21802.
76. Unger, T.; Wedler, S.; Kahle, F.-J.; Scherf, U.; Bässler, H.; Köhler, A., The Impact of Driving Force and Temperature on the Electron Transfer in Donor–Acceptor Blend Systems. *The Journal of Physical Chemistry C* **2017,** *121*, 22739-22752.
77. Grégoire, P.; Vella, E.; Dyson, M.; Bazán, C. M.; Leonelli, R.; Stingelin, N.; Stavrinou, P. N.; Bittner, E. R.; Silva, C., Excitonic Coupling Dominates the Homogeneous Photoluminescence Excitation Linewidth in Semicrystalline Polymeric Semiconductors. *Physical Review B* **2017,** *95*, 180201.
78. Dou, F.; Buchaca-Domingo, E.; Sakowicz, M.; Rezasoltani, E.; McCarthy-Ward, T.; Heeney, M.; Zhang, X.; Stingelin, N.; Silva, C., The Effect of Phase Morphology on the Nature of Long-Lived Charges in Semiconductor Polymer:Fullerene Systems. *Journal of Materials Chemistry C* **2015,** *3*, 3722-3729.